Supporting Information

Inherent Electrochemistry and Charge Transfer Properties of Few-Layer Two Dimensional $Ti_3C_2T_x$ MXene

Pranati Nayak,[a,b,⊥] Qiu Jiang,[a,⊥] Rajeshkumar Mohanraman,[a,⊥] Dalaver Anjum,[c] Mohamed Nejib Hedhili,[c] and Husam N. Alshareef[a]*

[a]*Materials Science and Engineering, Physical Sciences & Engineering Division,[c] Core Labs, King Abdullah University of Science and Technology (KAUST), Thuwal, 23955-6900, Saudi Arabia*
[b]*Electrodics and Electrocatalysis (EEC) Biosensor Division, CSIR- Central Electrochemical Research Institute (CSIR-CECRI), Karaikudi, Tamilnadu, 630006, India*

⊥These authors contributed equally to the work

*E-mail: husam.alshareef@kaust.edu.sa

Fig. S1 displays the basic characterizations of the parent Ti_3AlC_2 MAX phase and etched bulk-$Ti_3C_2T_x$ MXene. The FESEM micrograph of Ti_3AlC_2 MAX phase (Fig. S1a) shows compact, layered morphology. The layer separation in $Ti_3C_2T_x$ MXene is observed after chemical etching due to the removal of Al layers from parent Ti_3AlC_2 MAX phase (Fig. S1 b). The layer separation was confirmed again from high-resolution TEM image (Fig. S1c). The lattice resolved HRTEM image $Ti_3C_2T_x$ (Fig. S1d) shows the hexagonal lattice structure. The XRD patterns of Ti_3AlC_2 before and after LiF/HCl treatment are shown in Fig. S1(e). It can be seen in the XRD patterns that the crystallinity and structural order of Ti_3AlC_2 decrease after LiF/HCl treatment. As reported, the characteristic (002) peak at 9.5° 2θ in the Ti_3AlC_2 is broadened and obviously shifted to a much lower value, which results from the larger d-spacing and can be explained by the structural expansion from etching and substitution of Al with –F and –OH/=O terminating groups. The most intense peak at 2θ = 39° nearly disappeared, confirming the removal of Al layers from Ti_3AlC_2 which agrees with previous reports.[13, 4] Raman spectra of Ti_3AlC_2 before and after acid treatment are shown in Fig. S1 (f). Peaks ω_1, ω_3 and ω_4 assigned to Al-Ti vibration modes disappears after etching treatment. The peaks ω_5 and ω_6 appears with peak broadening and downshifting after etching, which is consistent with the literature. This fact confirms the loss of Al from the structure.[1]

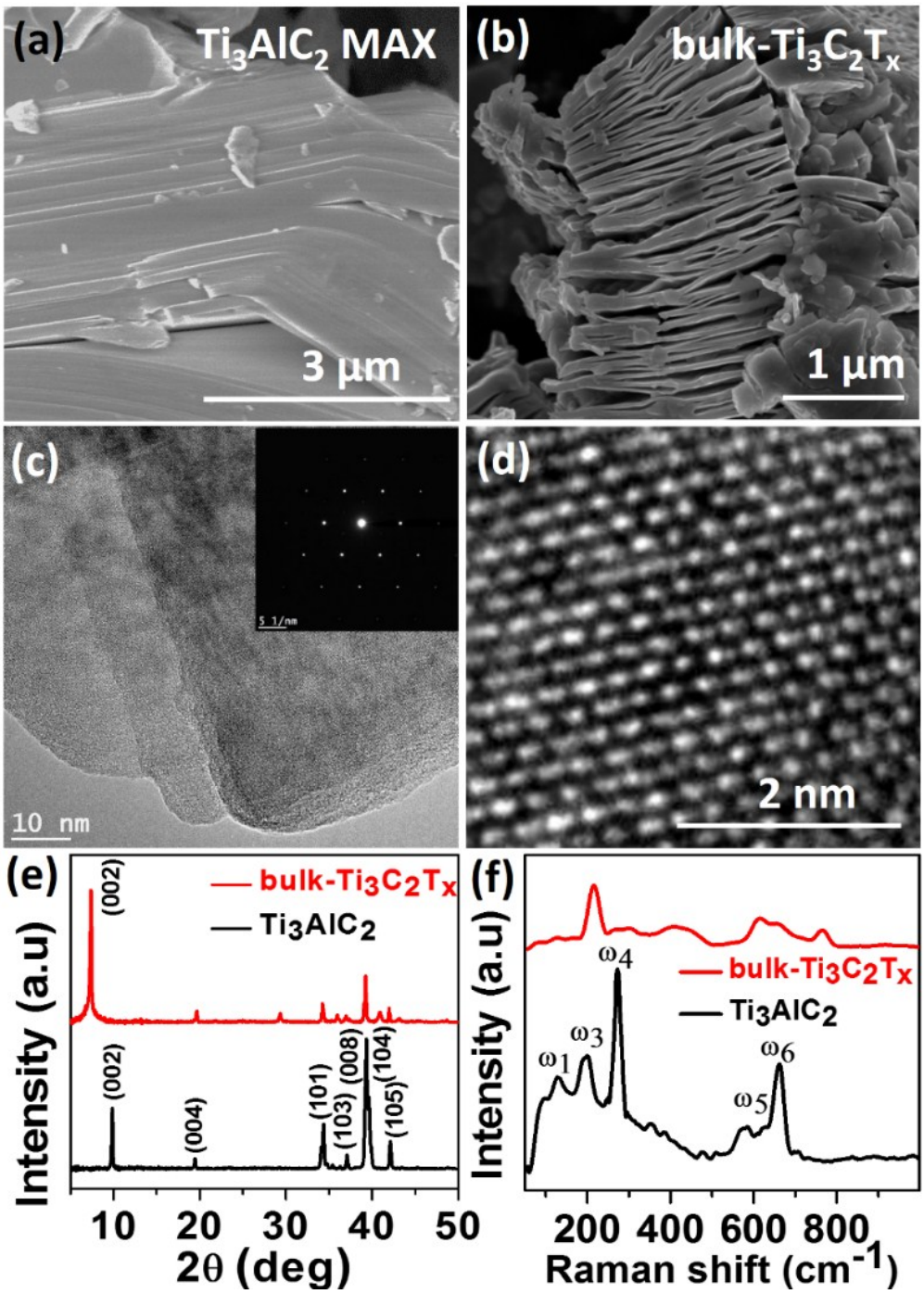

Fig. S1 FESEM image of (a) Ti_3AlC_2 MAX phase (b) bulk-$Ti_3C_2T_x$ MXene (c) TEM image (inset: selected area electron diffraction (SAED) pattern) (d) Lattice resolved HRTEM image of bulk-$Ti_3C_2T_x$ showing the Ti atom hexagonal lattice (e) X-ray diffractogram of bulk-$Ti_3C_2T_x$ MXene compared with parent MAX phase (f) Raman spectra of bulk-$Ti_3C_2T_x$ MXene compared with parent MAX phase.

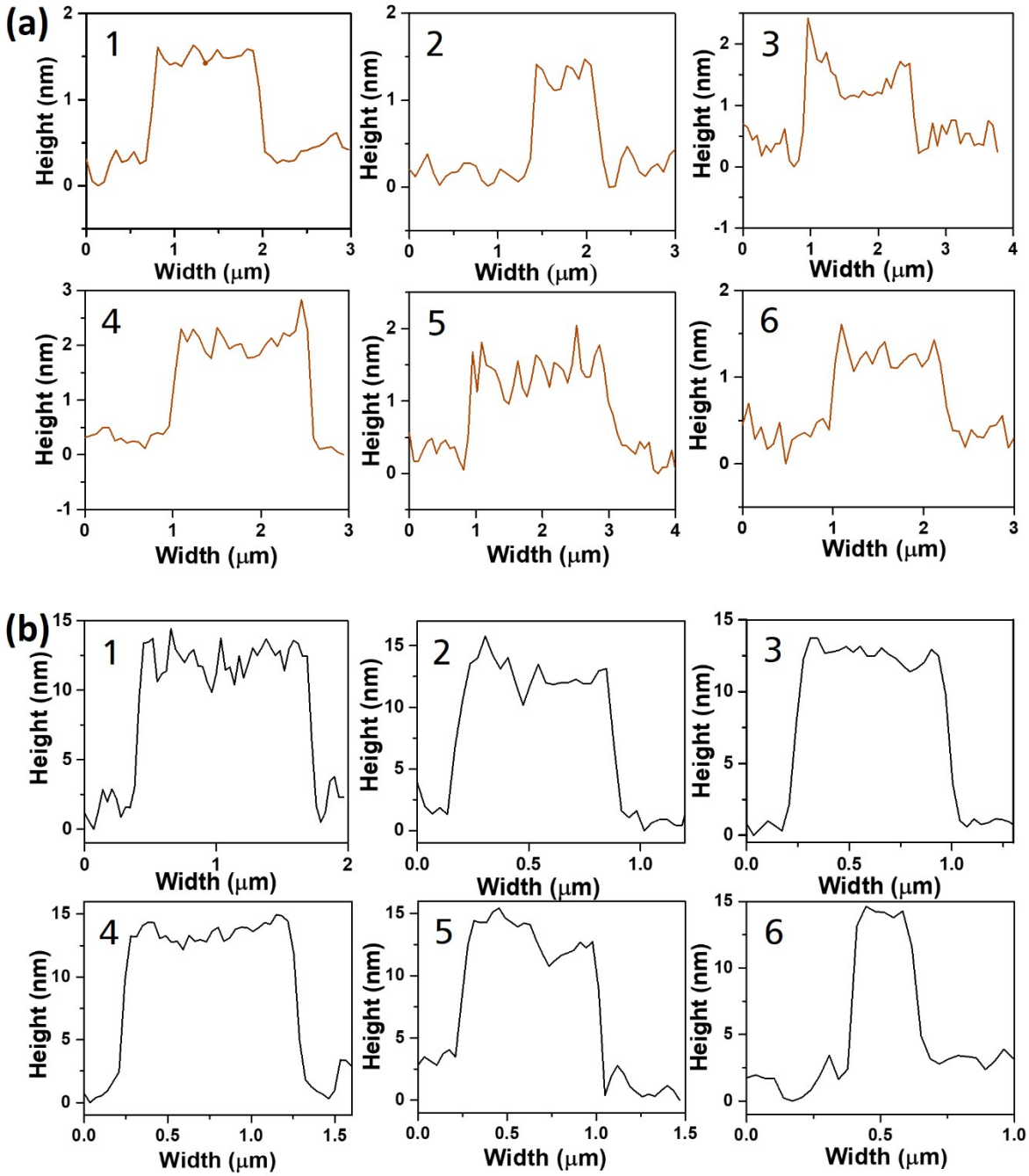

Fig. S2 AFM height profiles for (a) FL-$Ti_3C_2T_x$ and (b) ML-$Ti_3C_2T_x$ for six different flakes.

We conducted the XPS analysis of FL-$Ti_3C_2T_x$ and ML-$Ti_3C_2T_x$ in order to quantify the surface functionalities in both the materials. To be noted here, we adopted MILD method (12 M LiF + 9 M HCl) to prepare FL-$Ti_3C_2T_x$ and Clay method (5 M LiF + 6 M HCl) followed by ultrasonication to prepare ML-$Ti_3C_2T_x$. Fig. S3 shows the XPS survey and deconvoluted Ti 2p peak for (a, b) FL-$Ti_3C_2T_x$ and (c, d) ML-$Ti_3C_2T_x$ respectively. The elemental quantification is

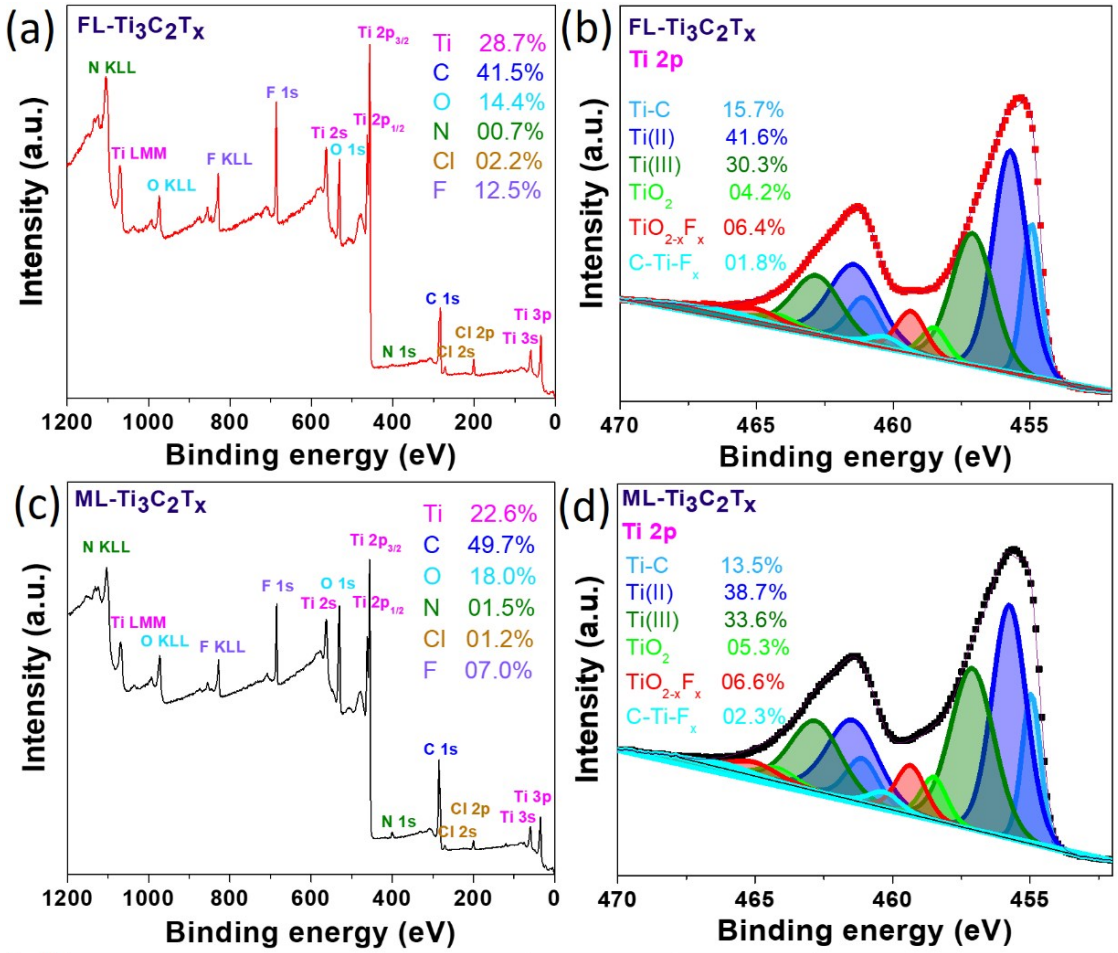

(e)

MXene	F	Cl	O	TiO_2	$TiO_{2-x}F_x$
FL-$Ti_3C_2T_x$ (12 M LiF/ 9 M HCl)	**12.5**	**2.2**	14.4	4.2	6.4
ML-$Ti_3C_2T_x$ (5 M LiF/ 6 M HCl)	7	1.2	**18**	**5.3**	**6.6**

Fig. S3 XPS survey spectra and deconvoluted XPS short scan of Ti 2p for (a, b) FL-$Ti_3C_2T_x$ and (c, d) ML-$Ti_3C_2T_x$, (e) table showing a comparison of surface functionalities of FL-$Ti_3C_2T_x$ and ML-$Ti_3C_2T_x$ MXene prepared by two different protocols.

shown in the insets of the corresponding figures. As observed, the content of F and Cl is higher in FL-$Ti_3C_2T_x$ compared to ML-$Ti_3C_2T_x$, which is obvious since the higher molar concentration of LiF and HCl were being used for FL-$Ti_3C_2T_x$ preparation. But TiO_2 concentration is little higher in ML-$Ti_3C_2T_x$ (5.3%) compared to FL-$Ti_3C_2T_x$ (4.2 %). This is quite obvious as bath sonication is involved in the preparation root. Even though we prepared ML-$Ti_3C_2T_x$ under highly controlled Ar flow and using a non-aqueous liquid for dispersion, a little enhancement

in oxidation is observed. Similarly, $TiO_{2-x}F_x$ is slightly higher in ML-$Ti_3C_2T_x$ (6.6%) compared to FL-$Ti_3C_2T_x$ (6.4%). This shows that the surface functionalities like surface oxides (TiO_2, $TiO_{2-x}F_x$) are slightly higher in ML-$Ti_3C_2T_x$, however, the functional groups like -F, -Cl concentration is slightly higher in FL-$Ti_3C_2T_x$. The percentage concentration of the deconvoluted Ti 2P peak is tabulated in Figure S3 e.

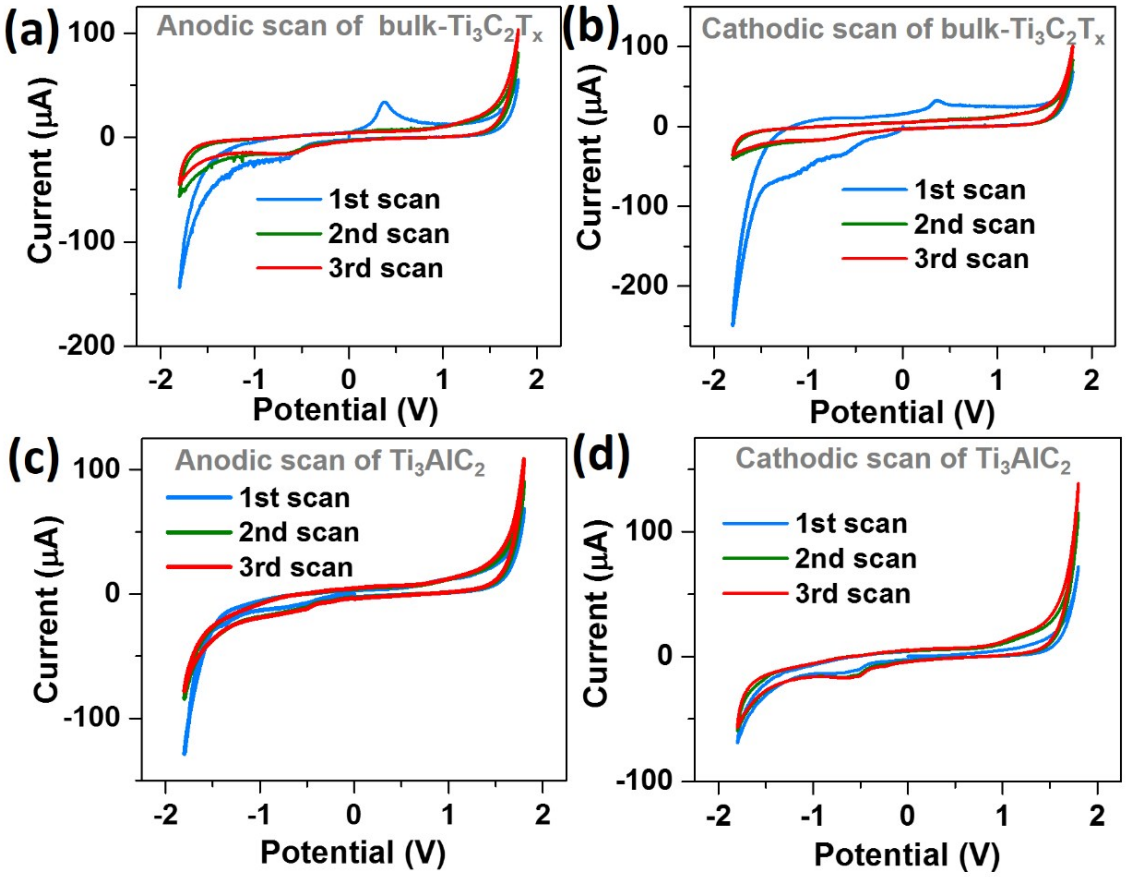

Fig. S4 Cyclic voltammograms of (a) $Ti_3C_2T_x$ MXene during anodic and (b) cathodic scan, (c) Ti_3AlC_2 MAX phase during anodic and (d) cathodic scan, Conditions: back ground electrolyte, PBS (0.1 M, pH 7.0); scan rate, 100 mV/s; all measurements are performed relative to the Ag/AgCl (1M KCl) reference electrode.

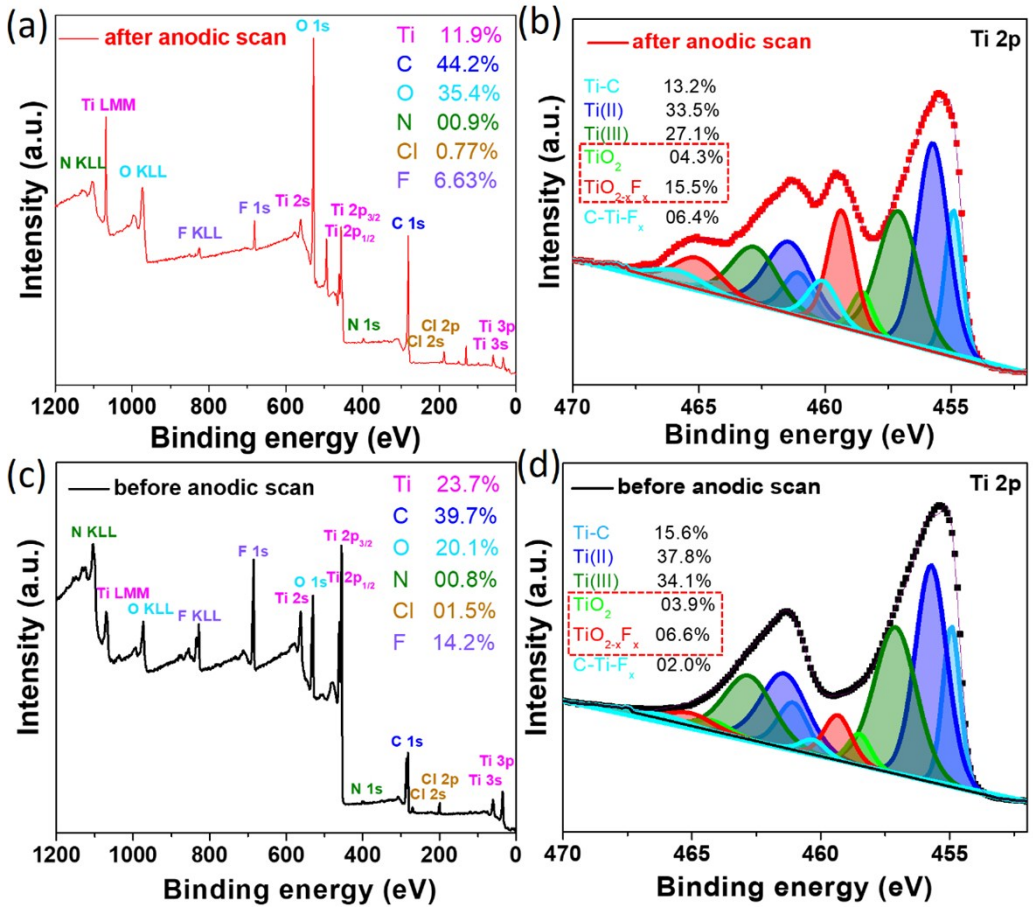

Fig. S5 XPS survey spectra and deconvoluted XPS short scan for Ti 2p in $Ti_3C_2T_x$ (a, b) after and (c, d) before conducting anodic scan.

Table S1 shows a comparison of surface functionalities of $Ti_3C_2T_x$ MXene before and after conducting anodic scan.

Region Ti $2p_{1/2, 3/2}$	BE (eV)	% Concentration	Assigned to
$Ti_3C_2T_x$	454.9 (461.0) 455.7 (461.4) 457.1 (462.8) 458.5 (464.2) 459.3 (465.0) 460.3 (466.0)	15.6 37.8 34.1 3.9 6.6 2	Ti-C Ti (II) Ti (III) TiO_2 $TiO_{2-x}F_x$ C-Ti-F_x
$Ti_3C_2T_x$ After anodic CV	454.9 (461.0) 455.7 (461.4) 457.1 (462.8) 458.5 (464.2) 459.3 (465.0) 460 (465.8)	13.2 33.5 27.1 4.3 15.5 6.4	Ti-C Ti (II) Ti (III) TiO_2 $TiO_{2-x}F_x$ C-Ti-F_x

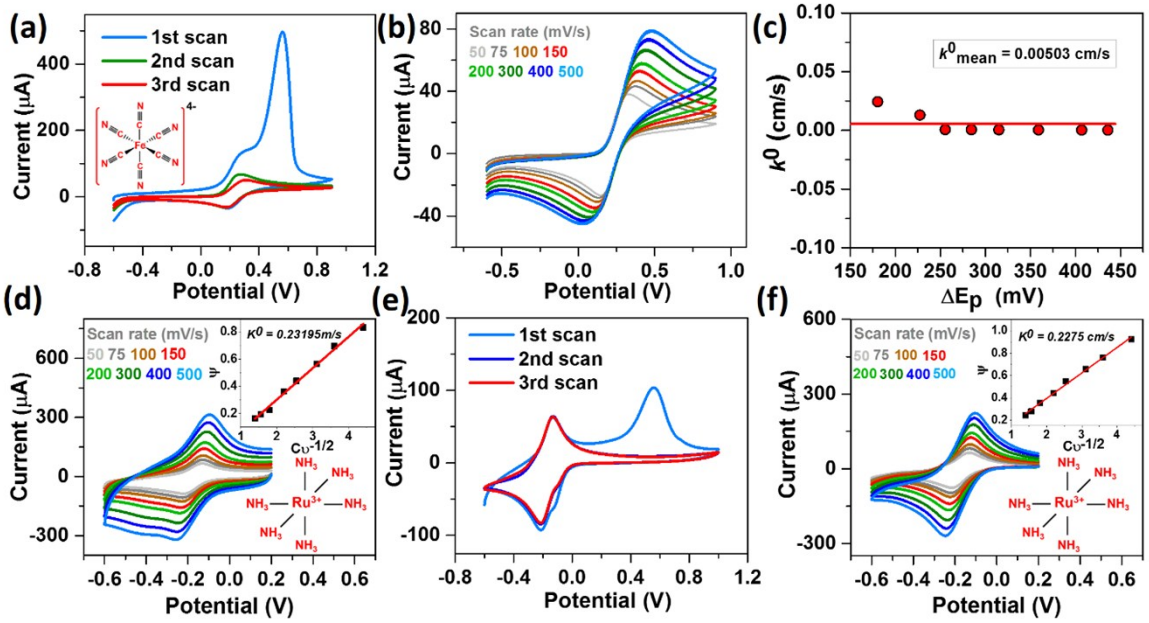

Fig. S6 Cyclic voltammograms of ML-$Ti_3C_2T_x$ MXene flakes recorded for 5 mM $[Fe(CN)_6]^{4-/3-}$ in 0.1 M KCl as supporting electrolyte; (a) initial three consecutive scans at 50 mV/s scan rate, (b) CVs at varying scan rates from 50-500 mV/s after recording 1st three scans. CVs recorded for 5 mM $[Ru(NH_3)_6]^{3+/2+}$ in 0.1 M KCl as supporting electrolyte at (d) scan rates rom 50-500 mV/s; (e) three consecutive scans recorded at 50 mV/s scan rate after recording (d); (f) again at varying scan rates from 50-500 mV/s. Corresponding Klingler-Kochi and Nicholson analyses and calculated HET rate (k^0) are shown in (c) and insets of (d and f).

Heterogeneous electron transfer (HET) rate

Since the peak-to-peak separation (ΔE) in the presence of the redox couple increase with scan rate ($\vartheta^{1/2}$), the reaction appears to be quasi-reversible in nature for both redox mediators (Fig. S6).[35] We employed the classical Nicholson method to calculate HET rate (k^0), which correlates the peak-to-peak separation (ΔE_p) to the charge transfer rate (k^0).[21]

$$\Psi = k^0\left(\frac{D_O}{D_R}\right)^{\frac{\alpha}{2}}\sqrt{\frac{RT}{\pi nFD_O\vartheta}} \qquad (1)$$

where ψ is the dimensionless kinetic parameter determined from ΔE_p and is proportional to D_O/D_R-the diffusion coefficient of the oxidized/reduced form of the electroactive species, α - the transfer coefficient, n -the number of electrons transferred in the electrochemical reaction, F -the Faraday constant (F = 96489 C/mol), ϑ -the scan rate in V/s, R - the universal gas

constant (8.314 J/K mol) and T -the absolute temperature. k^0 can be determined from the slope of Ψ vs. $C\vartheta^{-1/2}$ plot.

The method developed by Nicholson to calculate k^0 is limited to ΔE_p below 220 mV under the assumption of quasi-reversibility of the electrode reaction. If the irreversibility dominates (ΔE_p exceeds 220 mV) in the electrode reactions, a method developed by Klingler and Kochi is used for k^0 evaluation directly from the scan rate, ΔE_p and is reliable for $\Delta E_p \sim 150$ mV and beyond.[22, 23]

$$k^0 = 2.18\left(\frac{\alpha n F D \vartheta}{RT}\right)^{1/2} e^{-\left[\left(\alpha^2 F/RT\right) n \Delta E_p\right]} \quad (2)$$

Table S2

HET rate (k^0) of two redox mediators on different 2D materials of transition metal and noble metal chacogenide family before and after anodic scan compared with our results palladium telluride ($PdTe_2$) and platinum telluride ($PtTe_2$). Bulk molybdenum sulphide (MoS_2 (bulk)) and exfoliated molybdenum sulphide (MoS_2 (exfoliated)).

Materials	k^0 [cms^{-1}]				References
	$[Fe(CN)6]^{4-/3-}$		$[Ru(NH_3)_6]^{3+/2+}$		
	Before anodic scan	After anodic scan	Before anodic scan	After anodic scan	
$PdTe_2$ $PtTe_2$	6.5×10^{-5} 2.5×10^{-4}	3.4×10^{-6} 4.3×10^{-5}	- -	- -	33
MoS_2 (bulk) MoS_2 (exfoliated)	2.11×10^{-3} 2.26×10^{-4}	2.67×10^{-4} 2.50×10^{-4}	- -	- -	34
ML-$Ti_3C_2T_x$ **FL-$Ti_3C_2T_x$**	- -	**0.00503** **0.09533**	**0.23195** **0.399**	**0.2275** **0.383**	**This work**

Depending on the ΔE_p value, HET rate (k^0) was evaluated for both FL-$Ti_3C_2T_x$ and ML-$Ti_3C_2T_x$ electrodes. For $\Delta E_p <$ 220 mV, equation 1 was used to calculate k^0 (all of $[Ru(NH_3)_6]^{3+/2+}$ (shown in insets of Fig. S6 d and f) and most of $[Fe(CN)_6]^{4-/3-}$ data). For $\Delta E_p >$ 220 mV, equation 2 was used for each scan rate and the arithmetic mean was obtained as shown in Fig. S6c. The calculated k^0 values are tabulated in Table S2.

Table S3

HET rate (k^0) of two redox mediators on different 2D materials of carbon, transition metal and noble metal chacogenide family. basal plane pyrolytic graphite (BPPG); edge plane pyrolytic graphite (EPPG); few-layer (termed quasi-) graphene grown via CVD (q-graphene); mono-layer graphene grown via CVD (m-graphene); laser induced graphene from GO (L-graphene); graphene grown on copper foil by chemical vapor deposition (CVD-Gr); polyhedral structure graphene (Q-graphene); laser scribed graphene (LSG), bulk molybdenum selenide ($MoSe_2$(bulk)), BuLi-exfoliated molybdenum selenide ($MoSe_2^{\dagger}$), MeLi-exfoliated molybdenum selenide ($MoSe_2^{*}$), Tantalum sulphide (Tl_2S), palladium telluride ($PdTe_2$) and platinum telluride ($PtTe_2$).

	Materials	k^0 [cms^{-1}]		References
		$Fe(CN)_6]^{4-/3-}$	$[Ru(NH_3)_6]^{3+/2+}$	
Carbon family	EPPG	0.022	0.0038	24
	BPPG	10^{-9}	0.00877	24
	q-graphene	-	0.00158	25
	m-graphene	-	0.0011	25
	Monolayer graphene	0.15×10^{-3}	0.31×10^{-4}	26
	L-graphene	0.02373	-	27
	CVD graphene	0.014	0.012	28
	Q-graphene	0.0186	0.0177	29
	LSG	0.1150	0.0868	30
Transition metal dichalcogenides	$MoSe_2$ (bulk)	2.7×10^{-5}		31
	$MoSe_2^{*}$	1.52×10^{-4}		
	$MoSe_2^{\dagger}$	9.17×10^{-4}		
	WSe_2(bulk)	5.48×10^{-5}		
	WSe_2^{*}	3.83×10^{-6}		
	$WSe_2^{\dagger}$	1.21×10^{-5}		
	WS_2(bulk)	3.40×10^{-7}		
	WS_2^{*}	3.60×10^{-7}		
	$WS_2^{\dagger}$	2.75×10^{-6}		
	Tl_2S	6.3×10^{-5}		32
Noble metal dichalcogenides	$PdTe_2$	6.5×10^{-5}		33
	$PtTe_2$	2.5×10^{-4}		